FLOMEKO 2003
11th IMEKO TC9 Conference on Flow Measurement
Groningen, NETHERLANDS, 12 - 14 May 2003

INVESTIGATION OF FLOW CONDITIONING IN PIPES

Gabriel Moniz Pereira, Bodo Mickan, Rainer Kramer, Dietrich Dopheide,
Department of Fluid Mechanics, Physikalisch- Technische Bundesanstalt, Braunschweig, Germany

Ernst von Lavante, Institute of Turbo machinery, University of Essen, Essen, Germany

Paper reference 038

1. Introduction

It is a well-known and recognised fact that the behaviour of flow rate and volume measuring devices can be affected very strongly by the flow conditions prevailing in their inlet pipe section. Disturbed velocity profiles caused by pipe configurations such as bends, headers, pressure regulators and convergent or divergent pipe sections in front of a flow meter can lead to deviations of the meter reading by up to several percents.

Thus, flow conditioning normally means the generation of fully developed flows in the inlet of meters to avoid installation effects. Since this is in practice not always possible, it is necessary to investigate the influence of flow perturbations to the behaviour of flow meters. Such investigations are normally part of pattern approval in legal metrology. Hence, in case of pattern approval flow conditioning means the generation of disturbed flows with a definite and reproducible level of perturbation. The International Organisation of Legal Metrology OIML defined therefore standard pipe configurations (e.g. in OIML Recommendation R 32 [1]) to perform perturbations test within pattern approvals.

The test configurations recommended by OIML were defined for applications in atmospheric air. The main reason for this narrowed view was the huge effort necessary to perform perturbation test under high pressure conditions. In praxis this leads to several problems, mainly if the meter under test (e.g. some ultra sonic meters) works only with high pressure gas or the meter behaviour have strong dependence on Reynolds number or pressure. In the first case the economic effort for pattern approval is very high and only a few test facilities are able to handle such configurations and in the second case it is a very sensitive question to transfer results from low pressure to high pressure conditions.

In this paper some results of investigation in the field of installation effects and flow conditioning done in PTB[1] [1-7] are shown concerning following points:

- differences of flow conditioning using real pipes under low and high pressure conditions,
- a new concept (perturbation plate) for generating definite disturbed flows which can easily performed under high pressure conditions and
- basic investigations to improve the application of CFD simulations to determine flow profiles from geometry of piping.

[1] The research project sponsored by the Deutscher Verein des Gas- und Wasserfaches (DVGW).

2. Flow conditioning using real pipes under low and high pressure conditions

As mentioned in the introduction there are standardised test configurations recommended by OIML. These are the so called Low-Level and High Level perturbations which are shown in *Fig. 1a*. The Low-Level perturbation consists of a straight pipe with $5D_1$ length, a double bend out of plane (bend radius 1,5 D_1) and a divergent section. The diameter step of the divergent section depends on the standardised nominal pipe diameters , e.g. 80 to 100 mm, 100 to 150 mm or 150 to 200 mm. The High-Level perturbation is similar to the Low-Level but a half moon plate are additional applied between the two bends to generate stronger perturbations.

Looking at the geometry of OIML test configurations we find some problems with the comparability of measurements with different nominal pipe diameters. The divergent section varies for every nominal pipe diameter because the diameter step is different. Therefore the flow conditions are not absolutely transferable from one diameter to the other. In addition the inlet of the bends is not isolated to upstream flow conditions, hence we will get different results depending on the conditions at the test facilities.

Additional to the OIML test configurations a normal double bend out of plane (Fig. 1b) was used in the investigation program of PTB, because this is an industrial standard and the application of such configurations in test facilities for high pressure gas was easier than OIML configurations. The inlet section of the double bend was defined as a straight pipe of a length of 10D with Zanker flow conditioner to be independent from the flow conditions of test facilities. The double bend was built up according to both DIN as well as ANSI what leads to small differences in the geometry[2].

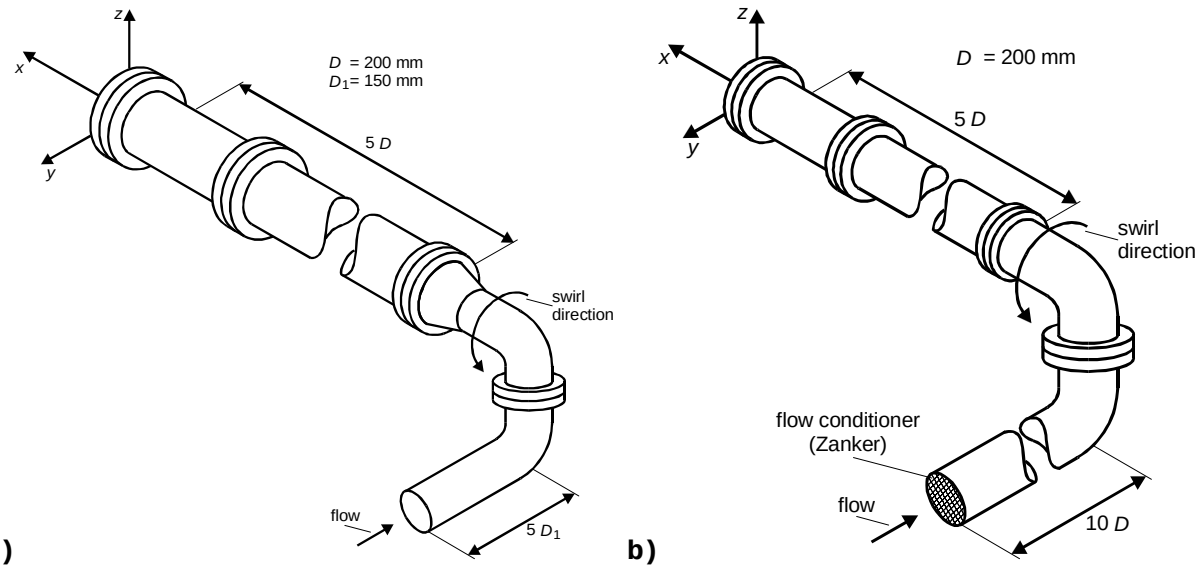

Fig. 1: *Examples of pipe configurations used to set up definite disturbed flow profiles:*
- *a) Standard test configuration OIML-Low-Level according to OIML recommendation R32; the OIML-High-Level configuration has additionally a half moon plate between the two bends.*
- *b) Double bend out of plane with bend radius 1,5 D. This configuration was used in the investigations of PTB because such kind of bend is an industrial standard. The inlet section was equipped with flow conditioner to be independent from upstream pipe configurations. According to OIML-High-Level configuration also a half moon plate between the two bends could be applied.*

[2] The length of straight pipe between the two bends is greater if ANSI flanges are used.

To carry out flow profile measurements an automated two-component Laser-Doppler velocity meter test facility for air measurements under atmospheric conditions was used [3]. This diagnostic test rig takes advantage of the construction of efficient miniaturised LDV [8] and the use of critical nozzles for the establishment of gas flow rate measurement of highest accuracy and reproducibility [9]. The test rig allows to measure two velocity components of in-situ flow profiles across the cross section in a DN 200 pipe at arbitrary inlet conditions. Up to now more than 250 hundred velocity profiles and the corresponding flow meter readings have been determined for different pipe configurations and flow conditioners at several flow rates [1-7].

For detailed analysis and comparison of flow profiles as shown in Fig. 2 and 3 it is necessary to quantify the main characteristics of the flow such as flatness, swirl and asymmetry by flow field parameters (profile numbers) and to compare the values of these profile numbers. In addition to this method a different way can be used by means of empirical models which describe the installation effects of a flow meter, if the parameters of these models are well chosen. This was done for orifice meters by Morrison [11] and for turbine meters by PTB [3].

In [12] e.g. a lot of different flow parameters have been discussed to describe velocity flow profiles. In the present case the flow profiles are characterised by defining three parameters [9]:

- The axial momentum number K_u:

$$K_u = \frac{\iint_A \rho u^2 r \, dA}{\pi \rho u_m^2 R^3} \tag{1}$$

  The closer the location of the flow to the wall the higher the momentum number of a pipe flow. Hence, a high momentum number indicates a flat axial velocity profile. A fully developed pipe flow has a certain momentum number $K_{uo} \approx 0{,}62$ but due to the fact that we are often interested only in the difference between a disturbed flow and the undisturbed case, we will use in the following also the difference $\Delta K_u = K_u - K_{uo}$.

- The swirl number K_w:

$$K_w = \frac{\iint_A \rho u w r \, dA}{\pi \rho u_m^2 R^3} \tag{2}$$

  The sign of the swirl number is related to the rotating direction of the swirl. Right hand swirls have positive, left hand swirls negative numbers.

- The asymmetry number K_A:

$$K_A = \frac{\sqrt{\left(y_S^2 + z_S^2\right)}}{R}$$

$$y_S = \frac{\iint_A y \cdot d\dot{m}}{\dot{m}} \quad \text{and} \quad z_S = \frac{\iint_A z \cdot d\dot{m}}{\dot{m}} \tag{3}$$

  The asymmetry is used to describe the distance of the centre of gravity of the mass flow from the pipe axis.

It was possible to quantify the disturbances of the flow profiles using these formulas (1) - (3) and it could be figured out to compare these disturbances (profile numbers) with the shift of the calibration curves (error shift) of turbine meters which were applied downstream of the

perturbation [3]. Detailed comparison of the profile catalogue (respective the profile numbers) with the measured error shift ΔE led to the empirical model:

$$\Delta E_{\text{model}} = a_1 K_v(1 + a_2 K_A) + a_3 \Delta K_u \qquad (4)$$

The model parameters a_1 to a_3 are characteristic for every turbine meter, and they have to be determined by regression from the profile numbers and error shifts.

Fig. 2 shows the axial velocity profiles measured 5 D downstream to OIML Low-Level configuration (Fig. 2a) and double bend out of plane (Fig 2b) according to Fig. 1. The comparison of both plots using the profile numbers indicates that the OIML configuration generates higher asymmetry (K_A) and flatness (K_u) of the axial flow.

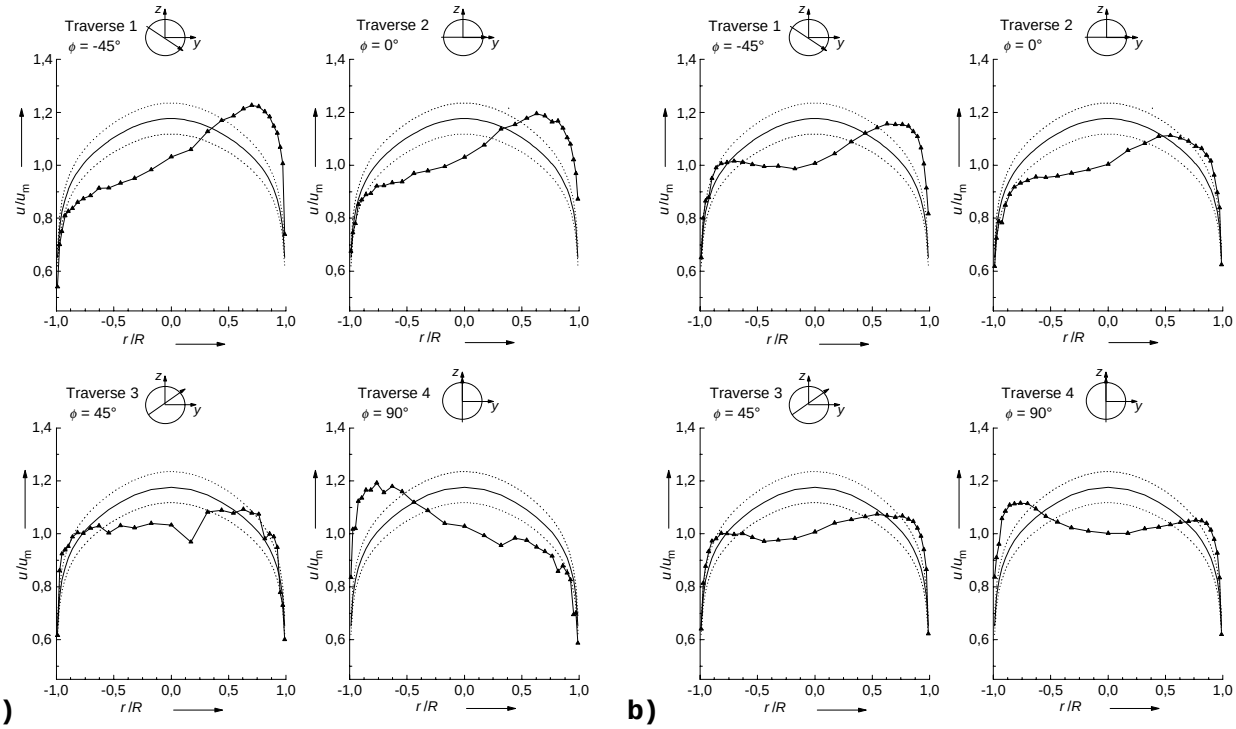

Fig. 2: *Axial velocity flow profiles measured with Laser-Doppler velocity meter:*
a) Downstream to OIML-Low-Level (see Fig.1a; distance 5D to perturbation).
Momentum number K_u: 0,682±0,008
Asymmetry number K_A: 0,081±0,017
b) Downstream to double bend (see Fig.1b; distance 5D to perturbation).
Momentum number K_u: 0,663±0,006
Asymmetry number K_A: 0,030±0,006

The tangential velocity profiles for the configurations of Fig. 1 are given in Fig. 3. In Fig 3a we found 5D downstream to OIML configuration a rotation of the gas similar to a solid body rotation. Downstream to the double bend (Fig 3b) the rotation is qualitatively the same but has more asymmetries. The strength of swirl (swirl number K_w) is in the case of OIML configuration a little bit higher. It can be shown by the law of conservation of momentum that the divergent section leads to an increase of swirl number up to the ratio of diameter step[3] D/D_1. This makes clear which problems are rising up from the geometry of OIML test

[3] Normally the increase caused by divergent section is a little bit smaller than the diameter step due to the dissipation of energy in the flow.

configuration if one want to compare results of measurements performed in two different nominal diameters.

Configurations with mirror symmetry to the configurations in Fig. 1 produce also flow profiles which have the same characteristics but mirror symmetry to Fig. 2 and 3 and the swirl rotates in contrary direction. Therefore the values of momentum number and asymmetry number as well as the absolute value of swirl number are the same.

In table 1 the values of profile numbers of several configurations generating swirl are given.

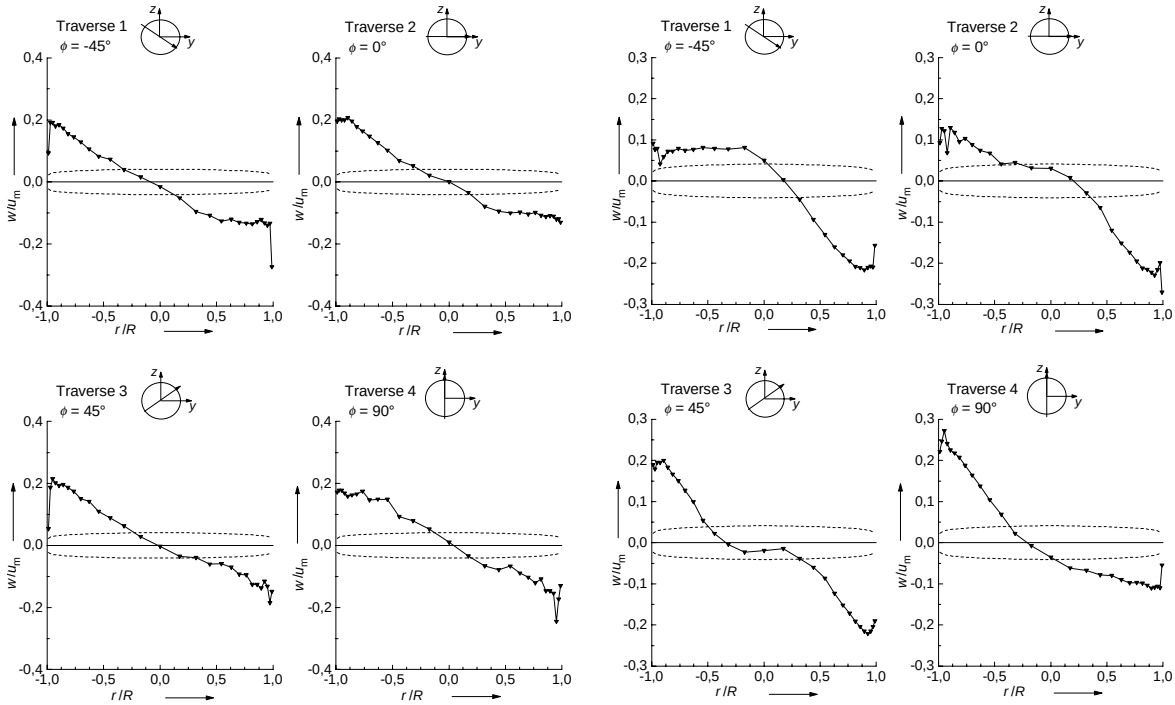

Fig. 3: *Tangential velocity flow profiles measured with Laser-Doppler velocity meter:*
a) Downstream to OIML-Low-Level (see Fig.1a; distance 5D to perturbation). Swirl number K_w: -0,115±0,009
b) Downstream to double bend (see Fig.1b; distance 5D to perturbation). Swirl number K_w: -0,092±0,007

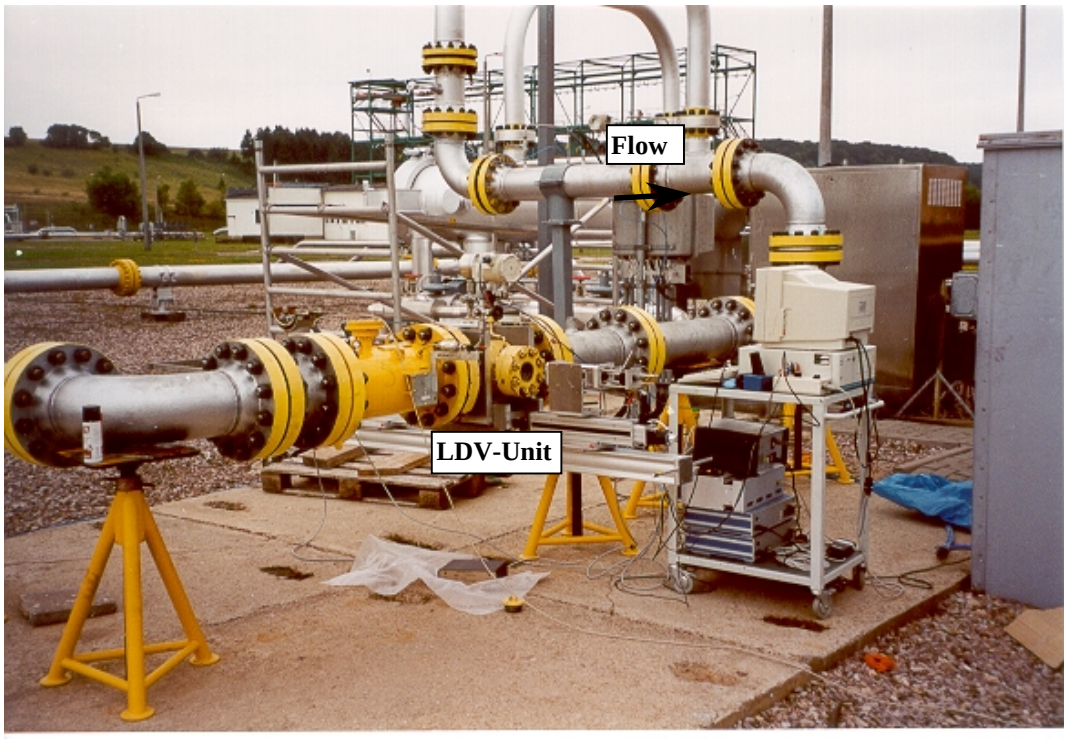

Fig. 4: *Photography of the high pressure test facility (42 bar) for profile measurements in natural gas* [4]

In the investigation program of PTB concerning installation effects the dependency of flow disturbances on Reynolds number was one of the main points of interest. The maximum Reynolds number possible at the test facility in PTB is about $Re \approx 6 \cdot 10^5$, but the most important application range of flow meters under high pressure gas are Reynolds numbers of several million. So it was necessary to perform profile measurements in this high *Re*-range to compare the results with atmospheric air.

For that purpose PTB built up a mobile LDV-unit which could be applied in pipes with flanges according to ANSI600. The test configuration investigated was the double bend in Fig. 1b again. Fig. 4 shoes a photo of the arrangement at the high pressure gas facility. It gives an impression of place necessary for investigation and the effort necessary for modifying such an installation. Therefore the number of profile measurements are much less than in atmospheric air.

The profile measurements for the double bend out of plane according to Fig 1b covered a range of $Re = 6 \cdot 10^3$ to $4 \cdot 10^6$. The profile numbers were determined for every flow profile measured and all results for the configuration with left hand swirl (i.e. negative values for K_w) are shown in Fig. 5. It can be observed that the absolute values of profile numbers decrease with the Reynolds number. But it is a surprising effect that there is a significant difference in momentum number and swirl number at $Re = 6 \cdot 10^5$ between measurements with air and natural gas.

[4] We acknowledge the gas supply company VNG AG for their very kind support of these measurements.

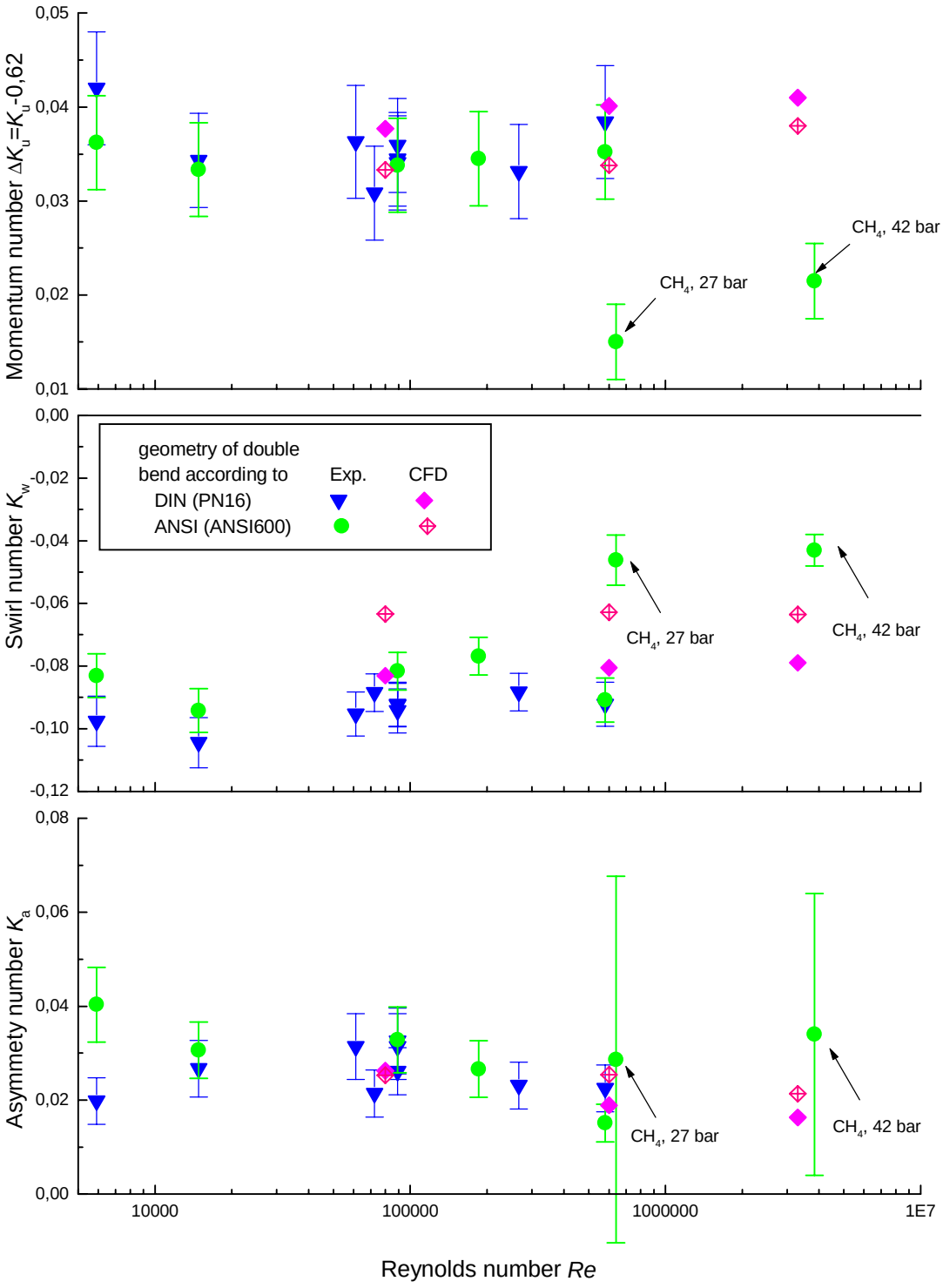

Fig. 5: *Dependency of profile numbers on Reynolds number. All profile numbers for $Re < 6 \cdot 10^5$ were determined from profiles measured in air at 1 bar. The profiles were measured with LDV 5D downstream to the configuration shown in Fig 1b. The configuration generates left hand swirl, therefore we get negative swirl numbers.*
There is a significant step in momentum number and swirl number between air and natural gas (CH_4) at the Re-number of $6 \cdot 10^5$, which could not realised in CFD.

Parallel to the experimental approach it was the aim to proof the application of CFD simulation[5] as a tool to underfeed rare experimental results. The outcomes of CFD simulation are also given in Fig. 5. The CFD simulations led generally to the same values as measured. But a detailed comparison of CFD with experiment shows two differences:

- CFD simulations shows greater differences between DIN- and ANSI-construction compared with experiment.
- There was no difference to be seen in CFD simulations at the same Reynolds number and different fluids as it was obtained in the experimental results.

The main characteristics for CFD used here are:

- CFD-Code: FLUENT V.5.4.8
- Turbulence model: k-ε model (Realizable k-ε -model)
- Near wall treatment: Standard wall function approach.
- Inlet boundary conditions imposed two pipe diameters upstream of configuration.
- Type of inlet boundary condition: Fully developed profiles of axial velocity component, turbulent kinetic energy k and turbulent dissipation rate ε. Fully developed conditions calculated from an asymptotic theory for Re-> infinity by Voigt [13]

At this stage it could not be the aim to demonstrate the fitting of CFD with experiments as good as possible. The character of experimental conditions and the materials used for investigations were industrial like and would not allow such purpose. From this point it can not compete with optimised conditions and results in a laboratory. The main points causing differences between numerical simulation and real flow might be:

- The shape of the cross section of the bends is in reality elliptic, what could not put into the geometry for simulation.
- It is difficult to determine the exact length of straight pipe between the two bends due to the ANSII600 welding flanges.
- The pipe was built up with different pieces. In praxis you will have problems with eccentricity and steps in diameter.
- The inlet flow to the bend was set by the Zanker flow conditioner nearly to fully developed conditions for the axial profile, but the turbulence structure of course will differ from that.

The difference in flow profiles (in profile number resp.) at the same Reynolds number for different fluid as air and natural gas seems to be unusual, but from the experiences with turbine meters such effects were not completely unknown (see Fig. 6 and 7). Therefore the relationship between error shift of meter and disturbed flow profile (given in equation 4) is helpful for this discussion.

[5] The CFD simulations were done by Ruhrgas AG [6].

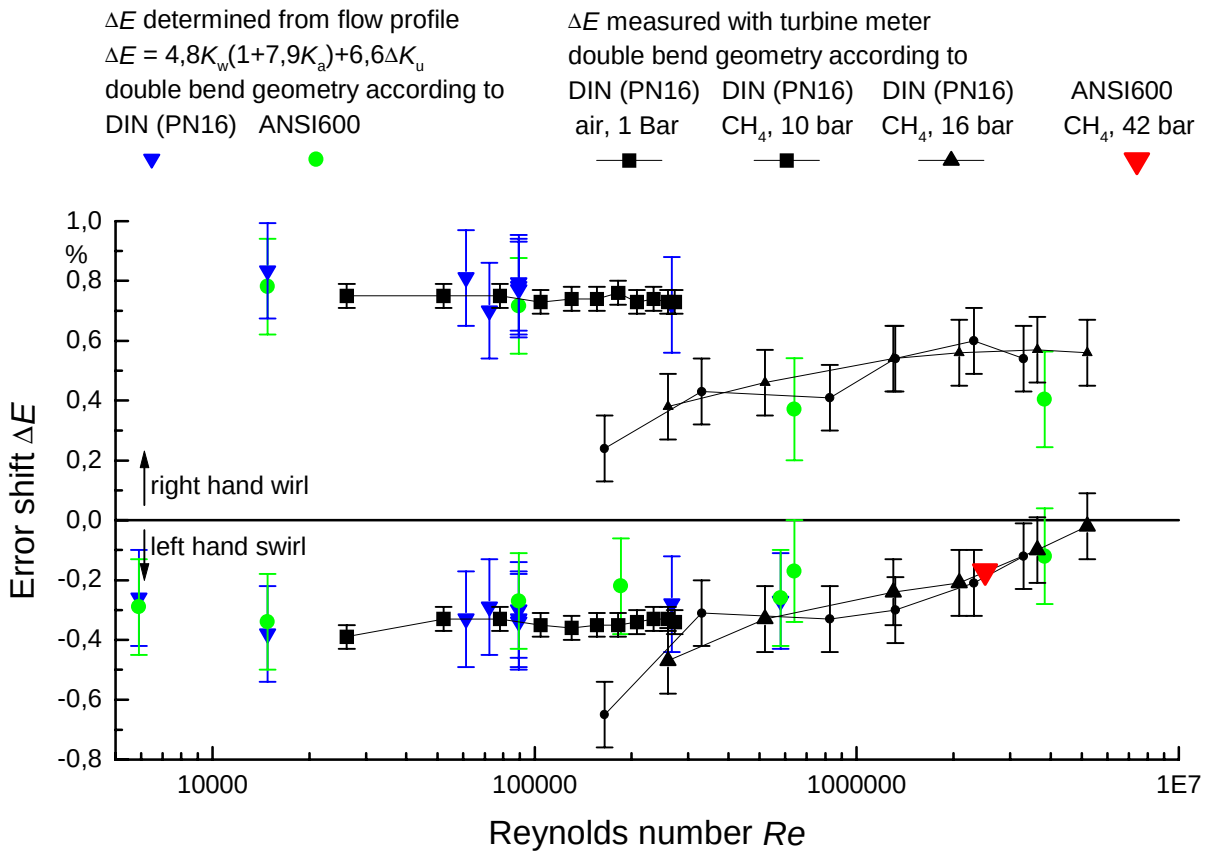

Fig. 6: *Error shift of a turbine meter. The meter was applied 5D downstream to configuration according Fig. 1b. The error shifts measured experimentally are compared with error shifts calculated with equation 5 (error shift model) using profile numbers of Fig. 5.*

The large data base of profile numbers correlated with error shifts led to the possibility to express the error shift in a empirical model according to equation 4 mentioned above. The turbine meter used here was extensively tested in different pipe configurations and the meter specific parameters of equation 4 were determined:

$$\Delta E = 4{,}8K_v(1 + 7{,}9K_A) + 6{,}6\Delta K_u \qquad (5)$$

It has to be emphasised that the parameters for this turbine meter were determined in former experiments with atmospheric air completely independent to the measurements in Fig. 5 and 6. Thus, the prediction of error shifts using results of Fig. 5 is a good possibility to proof the profile measurements.

In Fig. 6 the experimentally determined error shifts of a turbine meters are given which was applied 5 D downstream to the double bend. The turbine meter was used in air and natural gas in a Reynolds range from $Re = 2{,}5{\cdot}10^4$ to $5{\cdot}10^6$. Also the error shifts estimated from the measured flow profiles using equation 5 are shown. All results of error shifts have a high level of consistency concerning the uncertainties. Again a difference is to be seen in the overlapping range of the experiments with atmospheric air and natural gas under high pressure, especially for experiment with right hand swirl.

The measurements given in Fig. 7 have also a discrepancy between air and natural gas at same Reynolds numbers. But the results show additionally a strong dependency on Reynolds number caused by the meter. Hence, it is not always possible to conclude from the meter behaviour from low pressure to high pressure conditions. This underlines again the necessity of

perturbation test under high pressure conditions for pattern approval of new meter constructions.

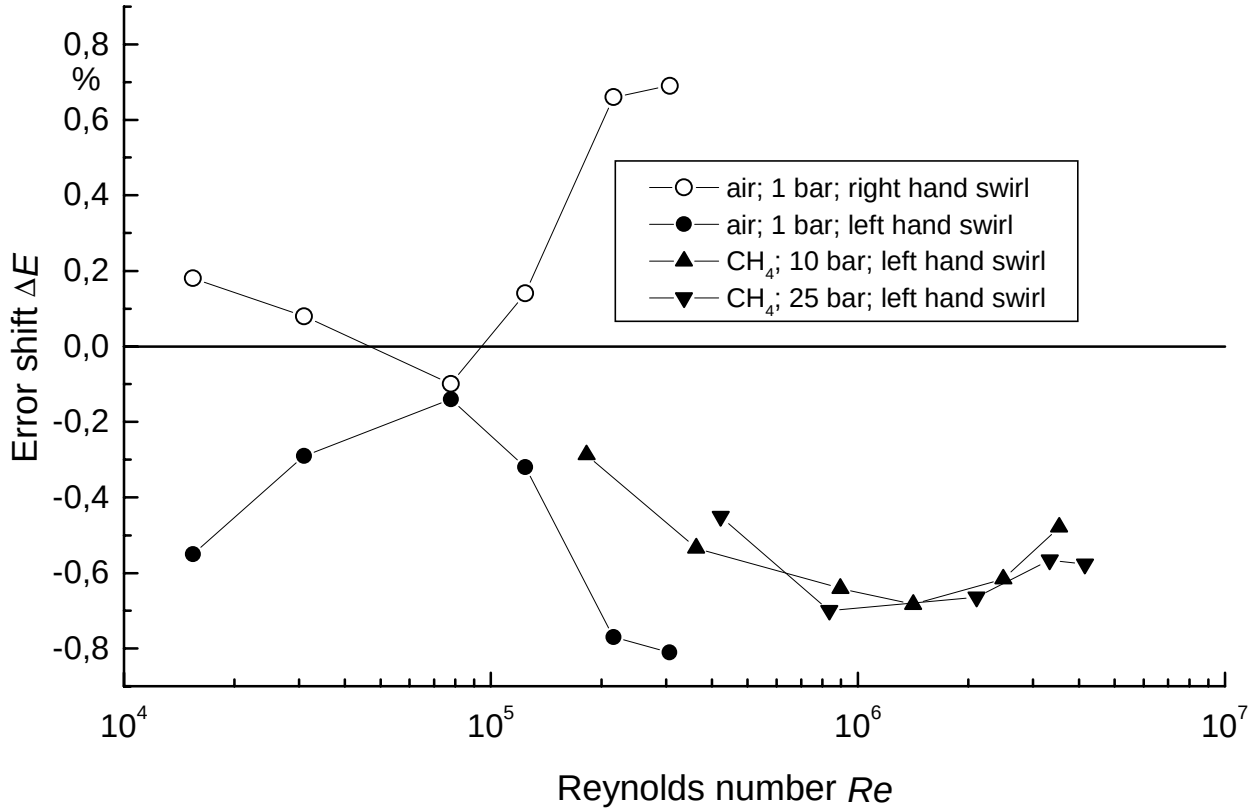

Fig. 7: *Error shift of a turbine meter with high Reynolds dependency. The meter was applied 5D downstream to flow conditions of configuration according Fig. 1a (OIML Low-Level).*[6]

[6] The results in Fig. 7 were determined within a research project of GERG; published in [10].

3. A new concept for the generation of disturbed flows: the perturbation plate.

As above mentioned the application of standard test configurations needs a huge effort under high pressure gas. Therefore a new way to set up definite flow conditions was gone in the PTB.

Outgoing from the experience with flow conditioners the development of the so called perturbation plate (see Fig. 8) was initiated. The main idea is a perforated plate, where the covered area is asymmetric to the pipe axis to induce asymmetries in the axial flow and the holes are drilled under an angle to the pipe axis to induce a swirl.

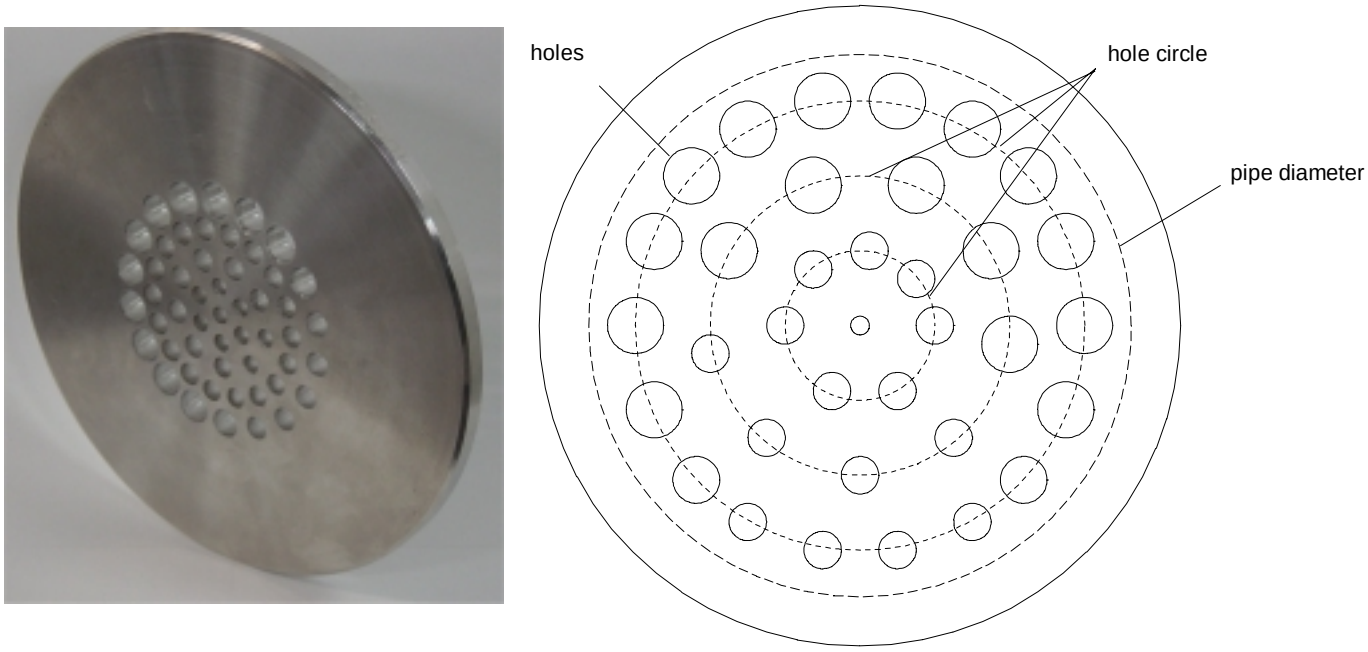

Fig.8: *Photography and outline of the perturbation Plate (PP) to induce definite asymmetries in axial flow and swirl. The drill axis of the holes is inclined to the pipe axis according to the strength of swirl.*

The application of the perturbation plate is as easy as of any flow conditioner. It can be placed between two flanges of a straight pipe in front of the meter under test. Only flow conditions near to fully developed flows are necessary in front of the perturbation plate. Therefore it is able to be applied in nearly every high pressure test facility for calibrations of meters under high pressure conditions. There is no need to change the piping of the test facility. Hence, the economic effort to perform perturbation tests is incomparable less then using the standard test configurations.

The strategy for the design of perturbation plate is very simple up to now. The diameter of the hole in the plate corresponds to the local velocity in the axial velocity profile downstream to the plate. The angle between drill axis and pipe axis is strongly related to the strength of swirl.

After the design of a prototype (as a first try) in the PTB two plates (PP I and PP II) are in use. These two plates generate the identical axial profile deformation and strength of swirl but the direction of swirl is different. Fig. 9 shows the measured velocity distribution downstream to PP I in atmospheric air.

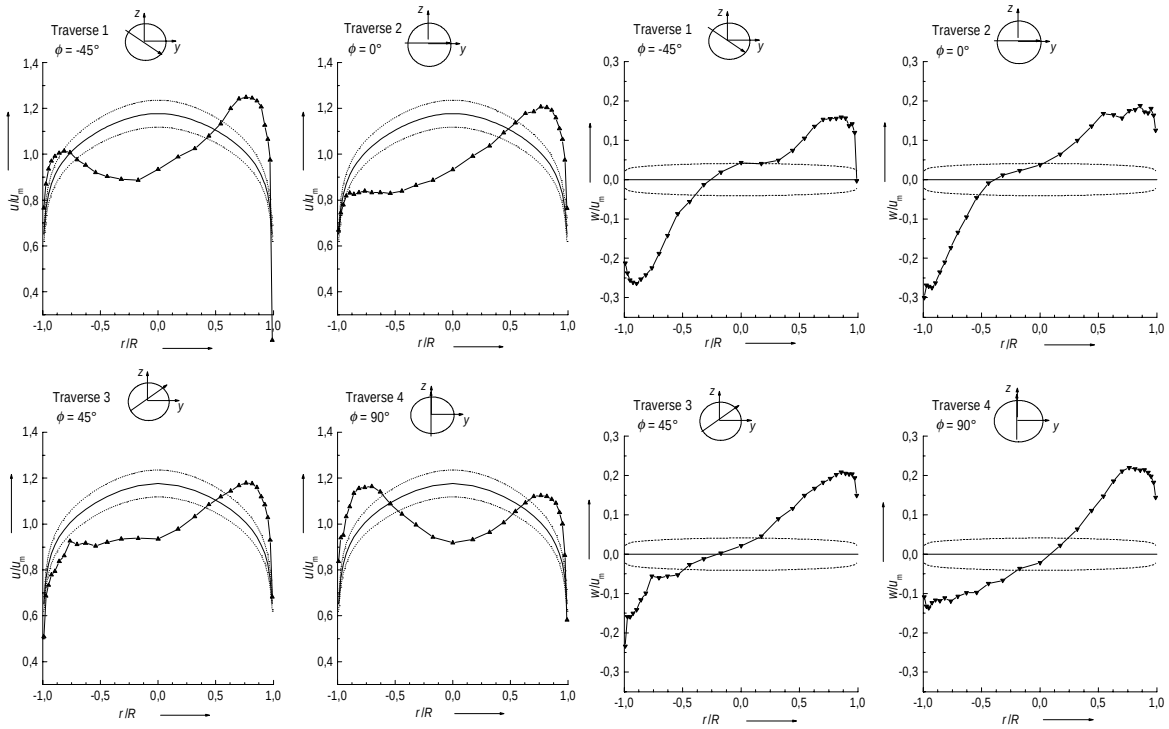

Fig. 9: *Velocity flow profiles downstream to perturbation plate PP I (distance 5D) measured with Laser-Doppler velocity meter (Re ≈ 10^5).*
a) Axial velocity:
Momentum number K_u: 0,682±0,005
Asymmetry number K_A: 0,050±0,010
b) Tangential velocity:
Swirl number K_w: 0,100±0,008

Comparing the quality of velocity distribution in Fig. 9 (PP I) and Fig. 2 and 3 (OIML Low-Level and standard double bend) a good similarity can be obtained. Using the profile numbers (giving in the figures and in table 1), the quantified comparison leads to the issue that the perturbation level of PP I and PP II is a mix of the OIML Low-Level perturbation and the double bend. The momentum number of PP I and PP II is nearly identical to OIML perturbation but the swirl and asymmetry numbers are in the middle of OIML Low-Level and double bend.

A further advantage of the perturbation plates for the application in high pressure gas is to be seen in the comparison of flow profiles measured in atmospheric air and natural gas at 42 bar (Fig. 10). Here the profiles are very similar to each other. In high pressure gas we see a little bit stronger swirl and flatter profile but the difference is not very significant. From this point we have a better chance to get comparable flow conditions between low and high pressure experiments than using real pipe configurations.

Table 1: *Profile numbers 5D downstream to perturbation plates and configurations generating swirl at Re ≈ 10^5 . The profile numbers were determined in pipe with a diameter of 200 mm.*

Configuration	Momentum number K_u	Swirl number K_w	Asymmetry number K_A	mean turb. level *Tu* (%)
double bend out of plane (bend radius 1,5 D, see Fig. 1b)	0,663±0,006	0,092±0,007	0,030±0,006	15
double bend out of plane with half moon plate between bends	0,661±0,005	0,142±0,011	0,038±0,008	25
OIML-Low-Level (see Fig. 1a)	0,682±0,008	0,115±0,009	0,081±0,017	20
OIML-High-Level	0,685±0,008	0,181±0,013	0,092±0,019	30
T-junction followed by bend	0,666±0,006	0,134±0,010	0,050±0,010	20
bend followed by T-junction	0,664±0,006	0,141±0,011	0,036±0,008	25
Perturbation plate (prototype) (left hand swirl)	0,684±0,008	-0,496±0,036	0,031±0,007	20
Perturbation plate **PP I** (right hand swirl)	0,682±0,005	0,100±0,008	0,050±0,010	20
Perturbation plate **PP II** (left hand swirl)	0,684±0,008	-0,100±0,008	0,060±0,012	20

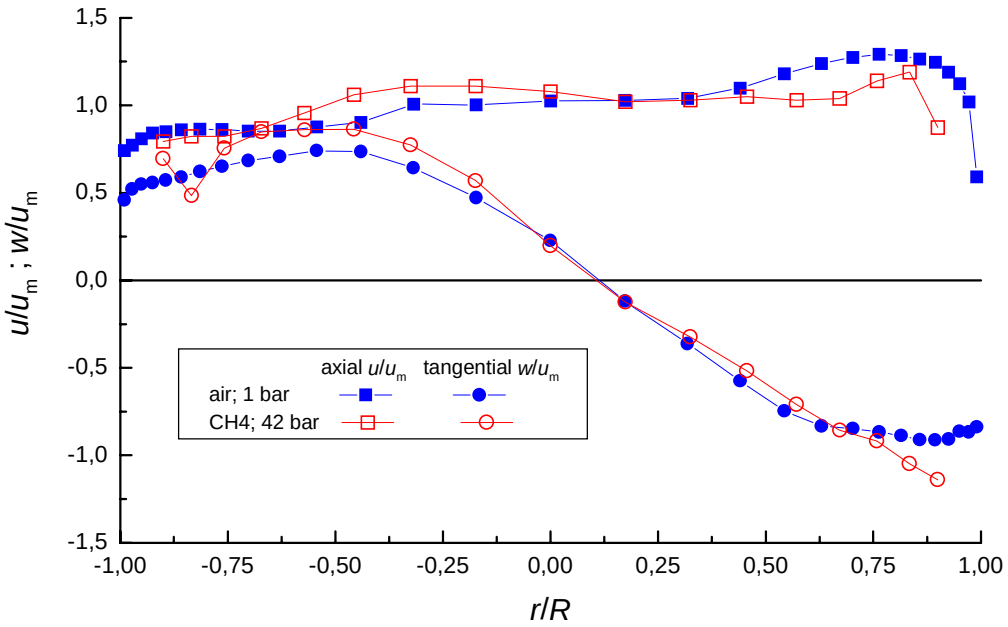

Fig. 10: *Velocity flow profiles downstream to perturbation plate PP prototype (distance 5D) measured with Laser-Doppler velocity meter in atmospheric air (Re ≈ 10^5) and high pressure natural gas at 42 bar (Re ≈ 3,6·10^6).*

Last but not least we want to compare of error shifts of a turbine meter applied 5D downstream to perturbation plates PP I and II as well as double bend out of plane (Fig 1b) in atmospheric air and natural high pressure gas. As aspects from the profile numbers the error shifts in atmospheric air are only slightly higher for the perturbation plates than for the double bend. But while the error shifts are increased for perturbation plates with the Reynolds number in contrary they are decreased for the double bend. Hence, the difference in high pressure gas between perturbation plate and double bend is much higher than in low pressure gas.

Up to now the perturbation plates were used in several pattern approvals for new ultrasonic flow meters. The producer of these meters decided by themselves to subject the meters to the stronger tests with the perturbation plates of current design under high pressure conditions. The advantage to get detailed information about meter behaviour from these investigations and to save money (compared with real pipe tests) is obviously a good argument for them.

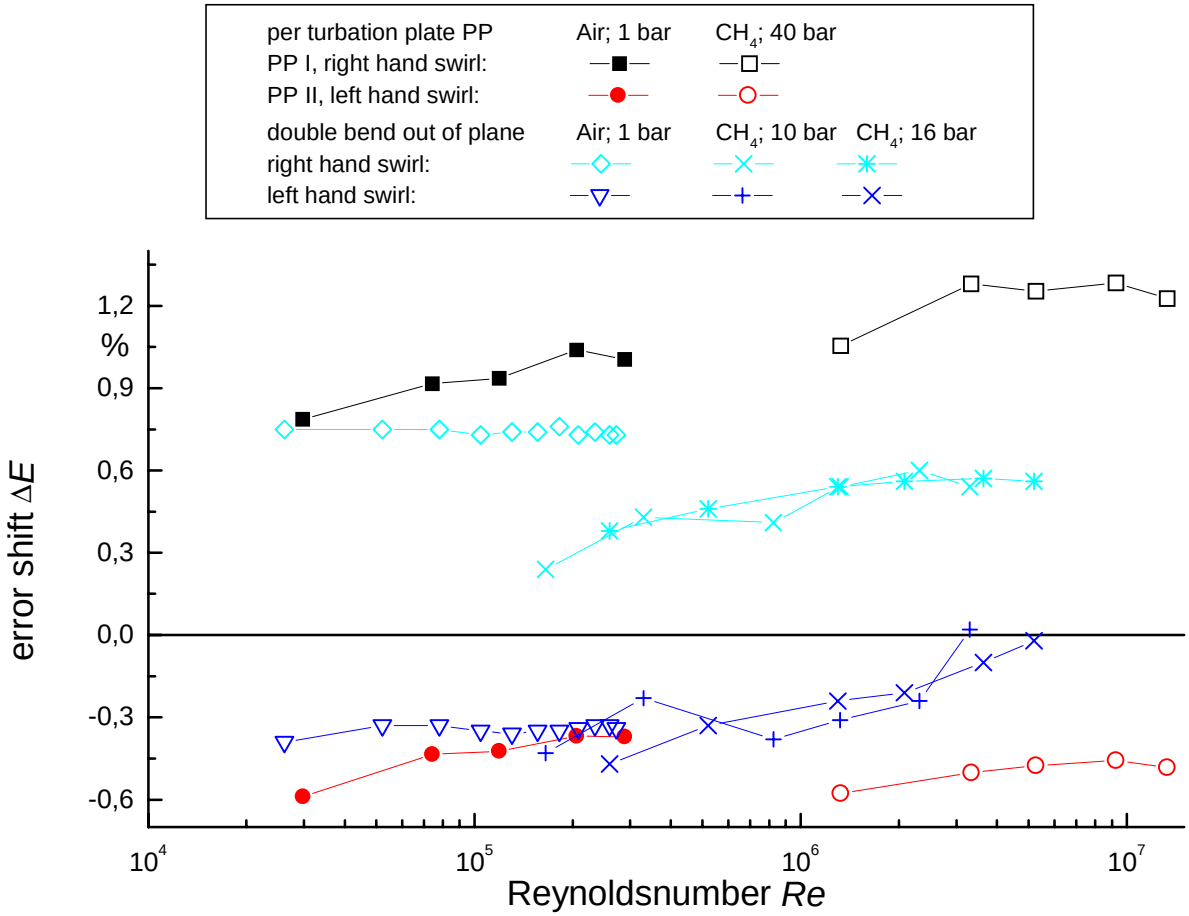

Fig. 11: *Comparison of error shifts of a turbine meter applied 5D downstream to perturbation plates PP I and II as well as double bend out of plane (Fig 1b) in atmospheric air and natural high pressure gas. The results for double bend out of plane are identical to the experimental results in Fig. 6.*

4. Preliminary summary

Up to here we could show in this paper different problems of flow conditioning using real pipes for investigation of installation effects and pattern approval. The main points can be summarised as follow:

- The pipe configurations recommended by OIML differ in their geometry from one nominal diameter to the other. Therefore it is difficult to compare the results of experiments performed in pipes with different diameters. Also the inlet conditions are not independent from the flow conditions of the test facility.
- There is not only Reynolds dependency of installation effects but also a dependency on other fluid properties. This can be observed in the measurement of velocity profiles as well in the reaction of flow meters to these profiles.
- Depending on the meter construction there can be an additional dependency on Reynolds number of the error shift of meter. Hence, the conclusion from meter behaviour in one Reynolds range to an other is not always possible and perturbation test shall be performed for new meter constructions in the Reynolds range of their application.
- To simplify the investigation of installation effects and to get better reproducibility, the so called perturbation plates were developed in PTB. Although there are up to now differences in the perturbation level downstream to the perturbation plates and real pipe configurations, some producers decided to use the advantages in current pattern approvals.

The performance of perturbation plates has to be improved especial for applications in high pressure gas. Therefore two points are actual under consideration:

- The knowledge of flow development downstream to the plates and real pipes should be better and
- we need new tools for designing a perturbation plate with a fine tuning of flow profile.

For both the application of CFD simulations would be helpful. The comparison of CFD results coming from commercial available programs with experimental results has shown that CFD simulations could not reflect all properties of the flow in pipes which were obtained from the experiment.

Outgoing from this, basis investigations of the behaviour of different numerical concepts were initiated at PTB to find the best CFD solution. The first results of these investigation are given in the following part of the paper.

5. Basic investigations to improve the application of CFD simulations

To produce a perforated plate of the desired properties, such as swirl generation and deformation of the axial flow profile nearly identical to e.g. double bends, a detailed knowledge of the physics in the *perturbation-plate* as well as local flow conditions is important. Here the CFD simulations should be used as comfortable tool.

To validate the CFD numerical results, the flow behaviour downstream of a sudden expansion in a pipe are investigated by measurements of velocity profiles and the static wall pressure.

As the turbulent backward facing step (axisymmetric case- sudden expansion in a pipe) is a typical flow with separation, further developments of turbulence models are tested on this flow case. Detailed flow measurements have been carried out, making evident the complex turbulent flow behaviour [16], [17], [18], [19].

It was necessary to proceed this way, as the CFD numerical simulations did not supply the measurements completely and in detail. Even the trends obtained in the experimental data could not always be seen in the results of numerical simulations.

The numerical simulations of the axisymmetric step-like enlargement are carried out using different mesh geometries, considering a variety of faces of the pipe expansion.

Various turbulence models are tested for the given cases in combination with different gas properties, assuming compressible and incompressible density of the used air flow medium.

5.1 Computational grids

The measurements were realised by using two different outlet configurations of the pipe expansion, shaped as a sharp edge as well as a chamfer of 2mm.

Considering the fact that both, an infinite sharp edge and a perfect chamfer are not realisable technically (Fig.13 a and b), four different outlet configurations were used to design the two-dimensional computational mesh geometry of the sudden expansion of the small 40mm pipe into a pipe of 206mm.

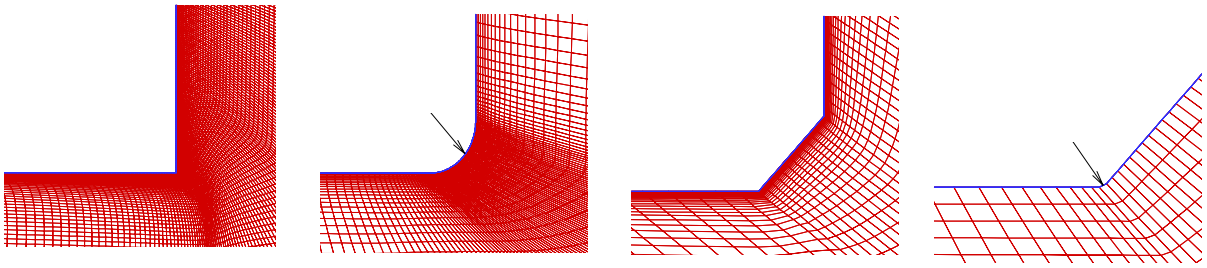

Fig.12: *2D Computational Meshes for numerical simulations (71952 Nodes, 71141 Cells)*

a) outlet 1	*b) outlet 2*	*c) outlet 3*	*d) outlet 4*
(sharp edge)	*(rounded edge, 50µm)*	*(chamfer, 2mm)*	*(rounded chamfer, 50µm)*

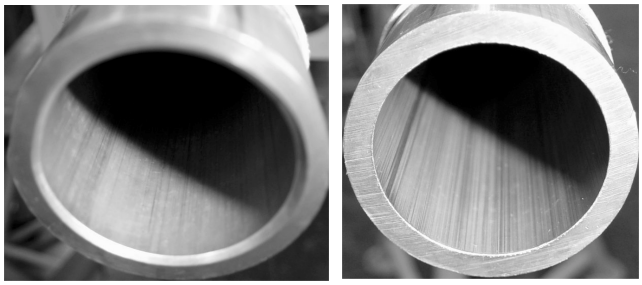

Fig.13: *Faces of the technical pipe expansion*
a) chamfer b) sharp edge

The outlet 1, assumed to have a sharp edge, and the outlet 3 having a non rounded chamfer of 2 mm represent idealised geometries, which are not realisable technically (Fig.12a, c). The rounded edge of 50µm radius represents the technical sharp edge and the rounded edges of the chamfer, rounded with 50 µm represents the technical. (Fig.12b, d).

Taking into account the numerical wall treatment and the boundary layers, different kind of meshes were created (table 2). The first kind of raw meshes consisted of 9964 Nodes and 9671 Cells. A finite-volume upwind solver, the commercial CFD Flow Modelling Software FLUENT was applied to carry out the spatial discretization of the governing equations [14], [15]. The standard wall function of this Software was used to resolute the viscous sub layer of this raw computational grids.

The turbulent flow of the sudden expansion in a pipe was modelled with different turbulence models, such as standard k-ε, RNG, RNG-differential, k-ε Realizable and Reynolds stress model.

All the computations with these turbulence models were combined with three different ways of calculating the density ρ of the air flow medium: constant, ideal and incompressible ideal gas.

The other kind of computational meshes consisted of 71952 Nodes and 71141 Cells. These fine computational grids do not need the utilisation of wall functions, since, more than 25 Cells were within the viscous sub layer and therefore the first cell is located at $y^+=1$.

5.2 Sudden expansion in a pipe - Measurements

Fig.14 shows the measured axial velocities of the sudden expansion of a circular pipe of radius R_1=0.02m with a chamfer as the face of the expansion into a pipe of radius R_2=0.103 m, having the radius ratio of $\beta=R_1/R_2$ =0.194175.

The examined volume rates are q_1=128.33 m^3/h and q_2=257.12 m^3/h. The measured mean velocities are u_{m1}=23.5 m/s (M_{a1}=0.07) and u_{m2}=57.5 m/s (M_{a2}=0.175), with the corresponding Reynolds numbers $Re_1= u_{m1}$ (2R DN40) / ν = 52 222 and $Re_2= u_{m2}$ (2R DN40) / ν = 127 777.

The separation point x_s of the flow coincides with the edge of the outlet of the smaller pipe at x=0 (Fig.14). The flow reattaches at the axial location x_r and redevelops downstream of the location of reattachment - if the pipe is long enough – to a fully developed turbulent state for the given Reynolds number. Although the mean velocity and the axial velocity profiles behind the reattachment location x_r appear to be fully developed it takes 100 – 200 lengths of the Radius R_2 of the bigger pipe to reach the fully developed axial velocity profile.

The most complicated zone to describe and the most difficult in which to make measurements was the reattachment location. Here, at any instant, the velocity displays large fluctuations in magnitude and may be positive or negative with respect to local mean velocity. The exact reattachment point x_r is difficult to measure.

Face of the expansion	*Nodes (Cells)*	*Inflow Conditions*	*Outflow Conditions*	*density*	*1st Cell*	*Near wall treatment*	*Turbulence model*
outlet 1, sharp edge	9964 (9671)	*velocity, mass-flow*	*pressure*	*constant ideal incompr.ideal*	$y^+ = 10$	*Standard wall function*	standard k-ε, RNG, RNG-differential, Realizable, Re- stress
outlet 2, rounded edge (50µm)	9964 (9671)	*velocity, mass-flow*	*pressure*	*constant ideal incompr.ideal*	$y^+ = 10$	*Standard wall function*	standard k-ε, RNG, RNG-differential, Realizable, Re- stress
outlet 3, chamfer 2mm	9964 (9671)	*velocity, mass-flow*	*pressure*	*constant ideal incompr.ideal*	$y^+ = 10$	*Standard wall function*	standard k-ε, RNG, RNG-differential, Realizable, Re- stress
outlet 4, rounded chamfer (50µm)	9964 (9671)	*velocity, mass-flow*	*pressure*	*constant ideal incompr.ideal*	$y^+ = 10$	*Standard wall function*	standard k-ε, RNG, RNG-differential, Realizable, Re- stress
outlet 1, sharp edge	71952 (71141)	*velocity, mass-flow*	*pressure*	*constant ideal*	$y^+ = 1$	*Resolution of viscous sub layer*	Realizable
outlet 2, rounded edge (50µm)	71952 (71141)	*velocity, mass-flow*	*pressure*	*constant ideal*	$y^+ = 1$	*Resolution of viscous sub layer*	Realizable
outlet 3, chamfer 2mm	71952 (71141)	*velocity, mass-flow*	*pressure*	*constant ideal*	$y^+ = 1$	*Resolution of viscous sub layer*	Realizable
outlet 4, rounded chamfer (50µm)	71952 (71141)	*velocity, mass-flow*	*pressure*	*constant ideal*	$y^+ = 1$	*Resolution of viscous sub layer*	Realizable

Table 2: *Parameters and Configurations of numerical simulations*

The averaged reattachment point was obtained with measurements of the static wall pressure and axial velocities by LDV (see the velocity profiles and the corresponding pressure coefficient in Fig.14).

The zone between the separation point and the reattachment x_r is bounded by the wall and the reattaching streamline Ψ_0. This zone is the largest segment of the separated region and is the so-called *recirculation zone*, where mean, back-flow velocities of order 0.1 u_m are measured.

The recirculation zone is divided into a forward and backward flow by the curve of location of the zero velocity line. Fig.14 shows the measured axial velocity profiles, the course of location of the zero velocity u_{z1} and the reattachment location streamline Ψ_0.

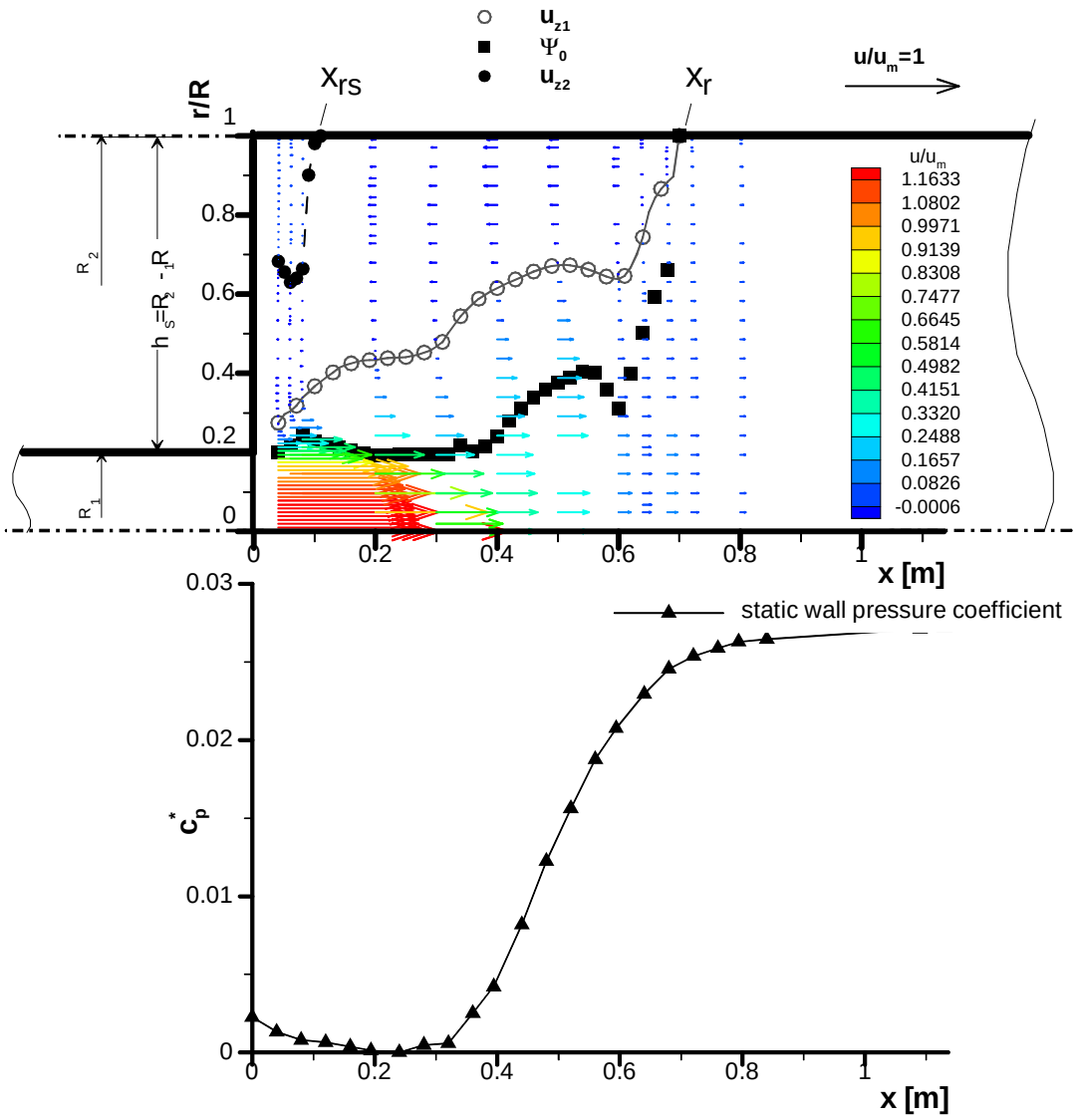

Fig.14: *Measured axial velocity profiles (*Re_2=127 777*), zero velocities* u_{z1}, u_{z2} *(of recirculation zone, corner eddy) and reattachment* x_r, x_{rs}, *reattachment location streamline* Ψ_0 *and normalised static wall pressure coefficient* c^*_p

There is also a second curve of location of zero velocity u_{z2} between the separation point x_s=0 and x_{rs}=0.1m. This *corner eddy* of exceedingly slow speed (0.01 u_m) can be seen between the face of the expansion and the reseparation point x_{rs} and always exists because of the slow back-flow velocity and because of the pressure gradient.

A typical curve of the normalised static wall pressure coefficient

$$c^*_p = (c_p - c_{p\min}) \cdot (1 - c_{p\min})^{-1}$$

versus distance from the step face is shown in the lower portion of Fig.14. In the investigated cases the transverse (radial) static pressure gradients are negligible compared to axial gradients.

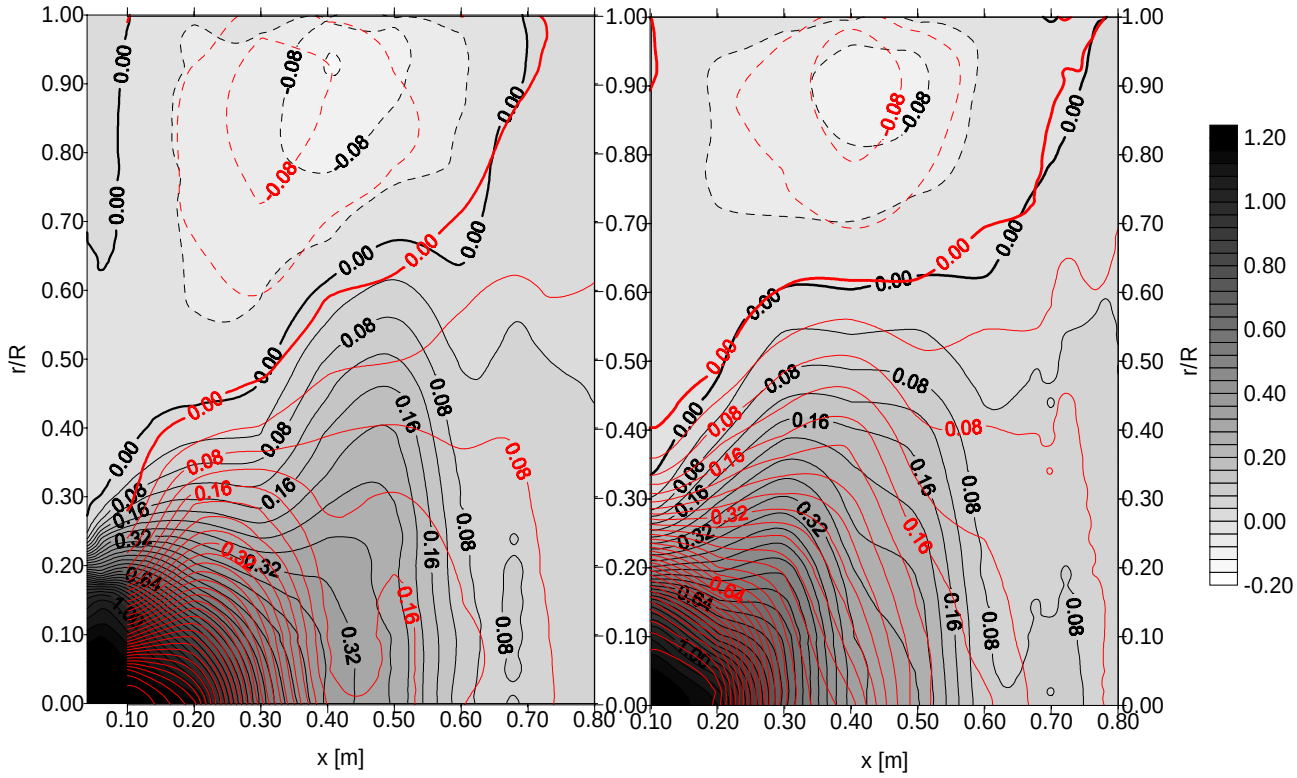

Fig.15: *Comparison of measured axial velocities, reattachment location points, recirculation zone, corner eddy, zero velocities for the flow rates q_1=128.33 m^3/h (red lines) and q_2=257.12 m^3/h (grey contours and black lines) for the face of the expansion with a) technical chamfer b) technical sharp edge*

Fig.15a compares the lines of constant axial velocity, reattachment location point, recirculation zone and the corner eddy with the corresponding curve of location of the zero velocities for the two different measured flow rates q_1 and q_2 of the chamfered face of the expansion.

The same results of the sharp edge are represented in Fig.15b. As the measurements of the velocity profiles start at x=0.1m and x=0.04m respectively (because of technical reasons), the existing corner eddies are not visible at all in Fig.15, but always present for both edge geometries and flow rates. The measured axial velocities for two different Reynolds numbers prove that the recirculation zone ends at nearly the same reattachment location point x_r of the respective outlet geometry, independently of the mean velocity u_m. Equally, the reattachment location streamlines Ψ_0 do not differ substantially and bound a recirculation zone of the same extension. The reattachment location points of the outlet with the chamfer are closer to the face of the expansion, with a lower pressure drop behind the recirculation zone.

5.3 Axisymmetric backward facing step - Numerical Approach

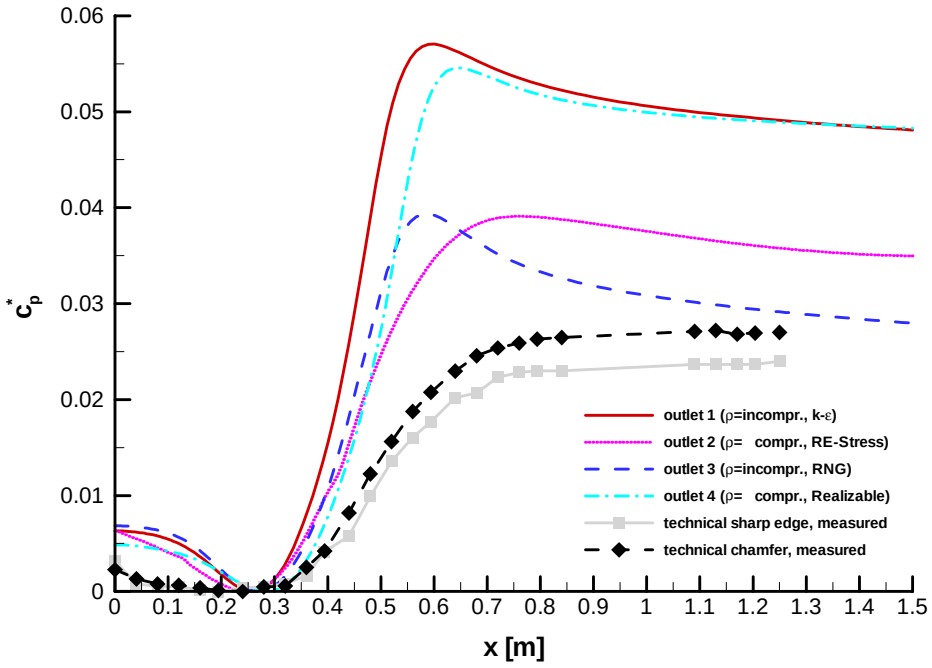

Fig.16: *Comparison of the best computed results with raw meshes of the normalised static wall pressure coefficient for different edge geometries and Turbulence models with measured results*

The first computations were carried out using raw computational grids (9964 Nodes and 9671 Cells), wherein the standard wall functions were used to resolute the viscous sub layer (table 2). Various Turbulence models with different gas properties were compared for all the outlet geometries. Fig.16 displays the normalised static wall pressure coefficient for the best numerical results, using different turbulence models and gas properties in comparison to the measured results of the technical chamfer and sharp edge.

To eliminate a possible influence of the wall functions used, further numerical simulations concentrated on the fine mesh geometry (71952 Nodes and 71141 Cells) with resolution of the viscous sub layer. The turbulence was modelled with the extended *realizable* k-ε turbulence model. The investigation concerning the gas properties was reduced to compressible and incompressible density gas.

Face of the expansion	x_r [m] reattachment	x_{rs} [m] reseparation	u_c (x=0.1m) core velocity	u_c (x=0.8m) core velocity	0.95 $c^*_p max$
Measurement technical sharp edge	*0.79*	*0.10*	*1.20*	*0.08*	*0.0228*
outlet 1, sharp edge (k-ε realizable, ρ=compressible)	0.59	0.11	1.03	0.04	0.0626
outlet 2, rounded edge (50μm) (k-ε realizable, ρ=compressible)	0.88	0.06	1.05	0.35	0.0605
outlet 2, rounded edge (50μm) (k-ε realizable, ρ=incompressible)	0.89	0.06	1.32	0.46	0.0930
Measurement technical chamfer	*0.70*	*0.11*	*1.20*	*0.07*	*0.0258*
outlet 3, chamfer 2mm (k-ε realizable, ρ=compressible)	0.60	0.11	1.01	0.04	0.0618
outlet 4, rounded chamfer (50μm) (k-ε realizable, ρ=compressible)	0.88	0.06	1.05	0.32	0.0602
outlet 4, rounded chamfer (50μm) (k-ε realizable, ρ=incompressible)	0.90	0.06	1.28	0.52	0.0925
outlet 4, rounded chamfer (50μm) (k-ε realizable, ρ=incompressible) [raw mesh with standard wall function]	0.64	0.01	0.96	0.03	0.0518

Table 3: *Comparison of x_r, x_{rs}, uc and $c^*_p max0.95$ for the flow rate q_2=257.12 m3/h (Re_2=127 777) for the measurements and chosen numerical results*

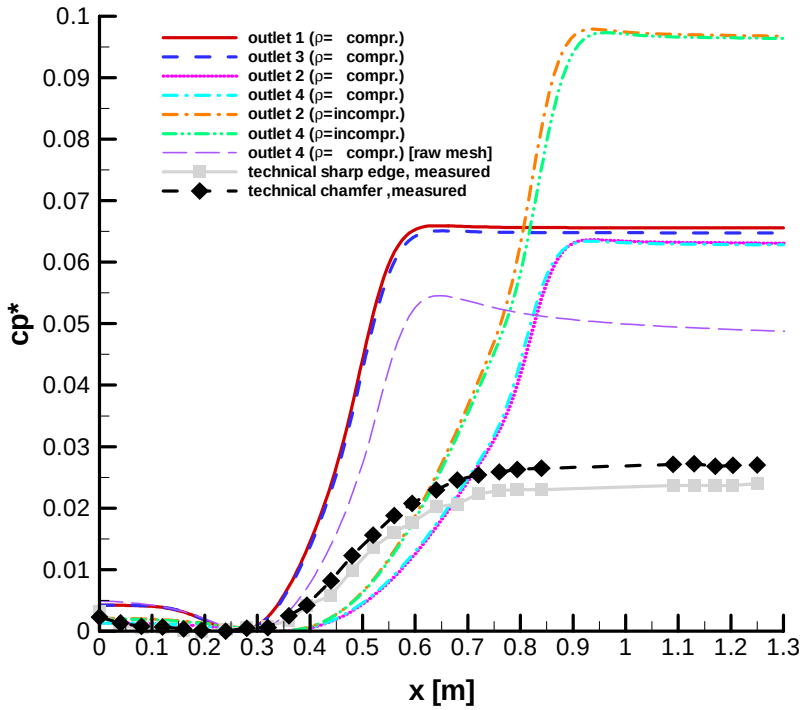

Fig.17: *Comparison of normalised static wall pressure coefficient for different edge geometries (fine mesh) and gas properties (k-ε realizable, turbulence model) with measured results*

Fig.17 points out the comparison of the CFD results and the measurements concerning the normalised static wall pressure coefficient. The measurements of c*p make clear that the pressure drop behind the recirculation zone of the outlet with a sharp edge is approximately 13% higher than the pressure drop of the edge with chamfer. In contrast to the measurements, no pressure drop, but a slight pressure gain is noticeable for the CFD results of computational meshes with a sharp and a rounded edge in comparison to the computational meshes of the chamfered edges.

In table 3 different parameters of measured and computed results are compared. The shown values are reattachment locations and reseparation points, core velocities at different distances to the face of the expansion and 0.95c*p max (95% of the maximum of normalised static wall pressure coefficient, where nearby the reattachment occurs).

As shown in Fig.17 and in table 3 predictions concerning static wall pressure, reattachment location and recirculation are very difficult for the investigated geometry.

There was no turbulence model currently used in a combination with the mesh geometry and gas density which adequately modelled the real flow.

The mean velocity u_{m1} =57.5 m/s corresponds to a Mach number of Ma_1 =0.175, so that the flow medium, as used, could be considered as incompressible for the numerical simulation.

The comparison of the normalised wall pressure coefficient c^*_p from the CFD results show, that the pressure levels behind the recirculation zone of the numerical simulations using incompressible gas are nearly 300% higher than the measured results and even 50 % higher than the simulations using compressible gas (Fig.17). In spite of a higher gradient of pressure drop behind the reattachment zone, the result obtained with the raw mesh, using standard wall functions is closer to the measured results than the values of the finer meshes.

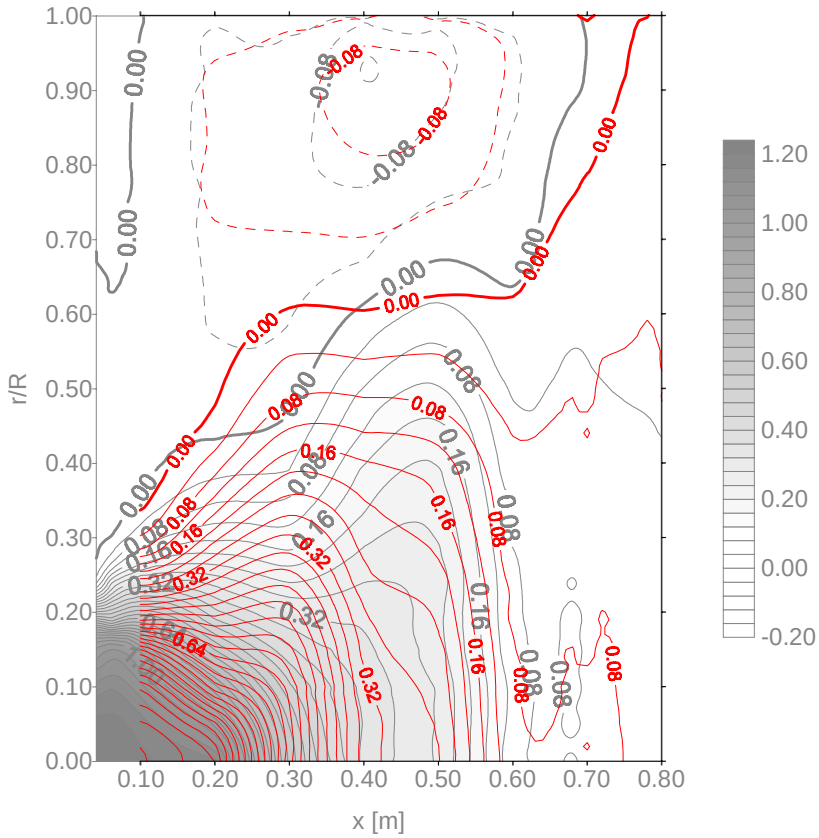

Fig.18: *Comparison of axial velocities, reattachment location points, recirculation zone, corner eddy and zero velocities for measured results of the face of the expansion with a) technical chamfer (grey contours) b) technical sharp edge (red lines)*

Fig.18 shows the measured results for the axial velocity of the two technical faces to the pipe expansion. In spite of the same extension of the recirculation zone, the reattachment occurs at different locations (table 3). The reattachment of the technical sharp edge at x_r=0.79 follows behind the reattachment of the chamfered edge at x_r=0.70. The velocity is almost equal along the core zone of the flow for both edges.

Fig.19 displays the numerical results of the rounded and sharp edge and Fig.20 shows the numerical results of the chamfer with and without rounded edges. The axial velocities of the rounded chamfer correspond to the results of the rounded edge and those of the sharp edge agree with the results of the non rounded chamfer. The extension of the recirculation zone, the velocity of the core zone and the reattachment location of the rounded edge and the rounded chamfer are nearly the same, as reflected by the static wall pressure (Fig.17) and the axial velocities shown in Fig.19 and Fig.20.

Similar results are obtained for the simple chamfer and the sharp edge.

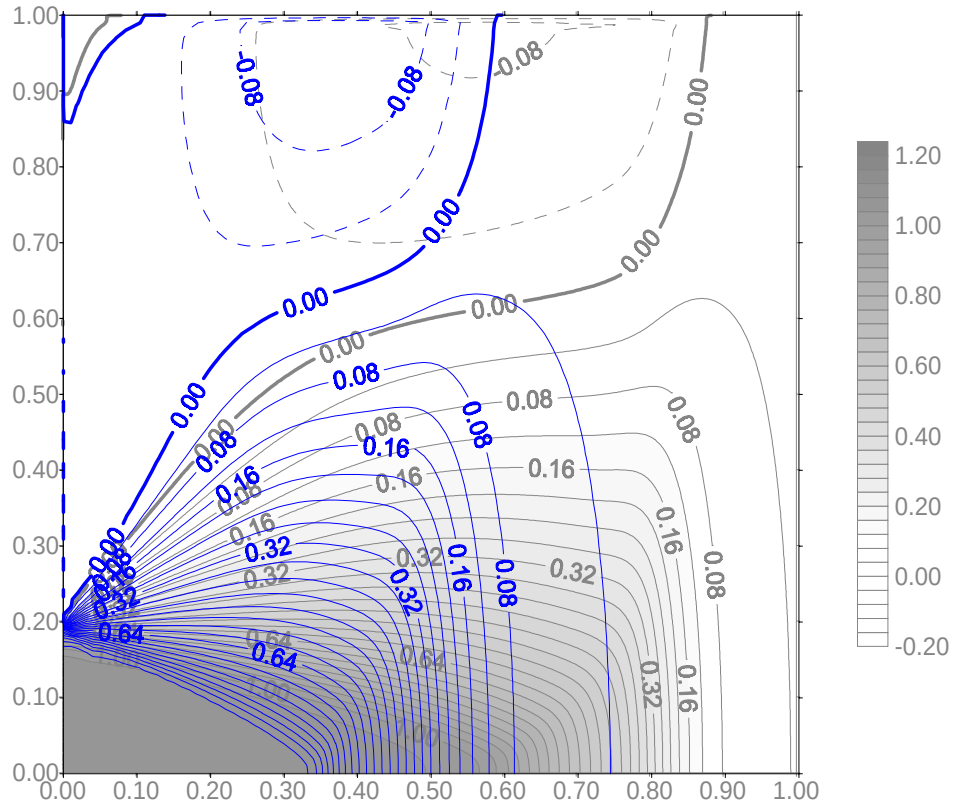

Fig.19: *Comparison of axial velocities, reattachment location points, recirculation zone, corner eddy and zero velocities for the numerical results of the face of the expansion with a) outlet 2, ρ=compr. (grey contours) b) outlet 1, ρ=compr. (blue lines)*

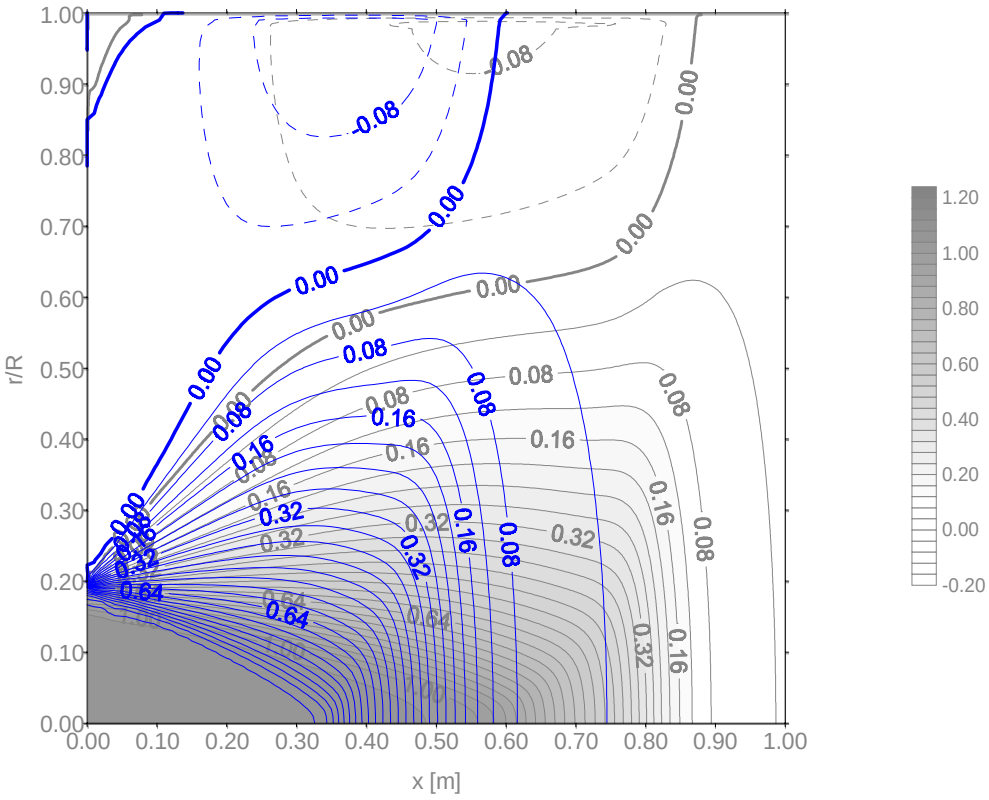

Fig.20: *Comparison of axial velocities, reattachment location points, recirculation zone, corner eddy and zero velocities for the numerical results of the face of the expansion with a) outlet 4, ρ=compr. (grey contours) b) outlet 3, ρ=compr. (blue lines)*

It is evident that the reattachment location x_r of the numerical simulations shown in Fig.19 and Fig.20 definitely depend on the computational mesh chosen. In contrast the selected model of the density did not affect the reattachment location x_r, but had a greater influence on the static wall pressure.

The numerical results obtained with rounded edge and rounded chamfer, respectively tend to a larger recirculation zone with a reattachment location at $x_r \approx 880$mm for both, compressible and incompressible gas.

The core velocities of all numerical results depend on the chosen density. The core velocities of compressible gas are 30% higher than those obtained with incompressible gas.

In comparison with the measured results, the recirculation zone of the computational meshes with chamfer and sharp edge are slightly smaller and the reattachment location points are located at $x_r \approx 600$mm. The attachment of the reseparation point of the corner eddy is located at $x_{rs} \approx 100$mm for the measurements, wherein the numerical results of the rounded faces of the extension compute a reseparation closer to the outlet at $x_{rs} \approx 60$mm. In contrast to, the non rounded faces of the outlet with a shorter recirculation zone cover a wider region with a reseparation located at $x_{rs} \approx 110$mm. The results of the raw mesh (table 3) show a small corner eddy ($x_{rs} \approx 10$mm) and also a smaller recirculation zone ($x_r \approx 640$ mm) with lower core velocities, but with better static wall pressure coefficient, in comparison with the measured results.

6. Conclusion and outlook

In the first part of the paper a representative selection of experimental results in the field of installation effects and flow conditioning in pipes have been presented. The discussion of these results figured out the problems of applications of real pipe configurations in high pressure natural gas compared to low pressure air (see also chapter 4. Preliminary summary). There was also shown the perturbation plate as a new and successful approach.

A comparison of detailed numerical simulations and measurements have been done with the aim of minimising the efforts of measurements. The first step was to use the most simply geometry related to our problem: the sudden expansion of a pipe. Preliminary results and the discussion have been outlined in the second part of this paper.

A distinct pressure difference behind the recirculation zone and different reattachment locations x_r were measured for the presently investigated chamfer as well as the sharp edge face expansion.

The results of the present 2D numerical simulation were not able to match the experimental data, although different mesh geometries of the face of the expansion, with different gas properties and different turbulence models were tried. At times, even the trends obtained in the experimental data could not be recovered.

The discrepancies concerning computed results depend on turbulence models used, the mesh geometries and the gas properties.

The dependence on the mesh geometry of the numerical results is evident and, consequently a fine tuning of the important parameters to the design of a perturbation plate for a certain flow case is practically feasible.

The tested turbulence models are sufficient for fast numerical computations and qualitative statements. The utilisation of wall functions avoids computational time consuming fine meshes (with a resolution of the viscous sub layer), consequently a speedup of the simulation is achieved.

A detailed investigation of the flow of the sudden expansion in a pipe and the two dimensional backward facing step respectively, is not feasible with vulgar k-ε turbulence modelling.

The reason of non-compliance is an assumed isotropy of turbulence by the tested turbulence models. A total anisotropy, a stretching of turbulence is a consequence of separation as well as recirculation and could not be compensated by changing parameters of the used turbulence models. The standard and modified k-ε turbulence models are not appropriate to resolute small vortices of turbulence.

As the measurements are extended to multiple jet expansions with shear-layer, interaction a two-dimensional numerical simulation is not suited to investigate the given case. Also, the present results show the necessity of improvement of turbulence modelling. A direct numerical simulation would be the best way to investigate all the flow phenomena to design the perturbation plate according to all demands. Because of the limitation of the computers nowadays, CFD results are only available for Reynolds numbers up to a maximum of 10000-20000. A simulation of flows of much higher Reynolds numbers would be almost impossible in the near future.

Hence, the numerical simulations have to be extended to three dimensions with appropriate turbulence modelling. That implies fine scale turbulence modelling using sub grid scale models by means of LES to resolve the swirl properties of the recirculation zone and turbulence structures correctly and to describe the separation and reattachment location in detail.

An extension of the present work to a bundle of multiple tubes with enhanced study of interaction of multiple jets is aimed and a successive reduction of the investigated tube diameter will result in step by step realisation of the configuration of the perturbation plate.

7. References

[1] International Recommendation: Rotary piston gas meters and turbine gas meters. (OIML R-32); Edition 1989 (E)

[2] G. Wendt, B. Mickan, R. Kramer and D. Dopheide (1996). Systematic investigation of pipe flows and installation effects using laser Doppler anemometry; Part I: Profile measurements downstream of several pipe configurations and flow conditioners. Flow Meas. Instrum., Vol. 7, (1996), No. 3/4, pp. 141-149

[3] B. Mickan, G. Wendt, R. Kramer and D. Dopheide (1996). Systematic investigation of pipe flows and installation effects using laser Doppler anemometry; Part II: The effect of disturbed flow profiles on turbine gas meters - a describing empirical model. Flow Meas. Instrum., Vol. 7, (1996), No. 3/4, pp. 151-160

[4] B. Mickan, G. Wendt, R. Kramer, D. Dopheide: "Installation Effects: Disturbed Flow Profiles, their Effect on Turbine Meter Performance and the Efficiency of Flow Straighteners" , Conference Proceedings International Gas Research Conference (IGRC98), San Diego, California (USA), 8.-11. November 1998, Printed Proceedings, Volume II: Transmission and Storage, Gas Research Institute, GRI-98/0226.2, TSO-10, p. 196-208

[5] B. Mickan, R. Kramer, G. Wendt, D. Dopheide: "Quantified comparison of the efficiency of new flow conditioners", 10th International Conference on Flow Measurement, FLOMEKO'2000, Salvador, Brazil, June 4-8, 2000, CD-ROM, Session A7

[6] B. Mickan, R. Kramer, H. Gehlhaar, A. Schmücker, D. Dopheide: "Installation Effects - A Comparison of Experimental Results with Atmospheric Air and High Pressure Natural Gas as well as Results of CFD", Flow Measurement 2001, Proceedings of International Conference, 7th - 10th May 2001, Peebles, Scotland, Published by National Engineering Laboratory (NEL), CD-ROM Session 5, p. 1-11

[7] R. Kramer: "Investigation of flow profiles in pipes based on the Laser Doppler Velocimetry", Conference Proceeding, Metrologia 2001, Czech Gas and Oil Association, 14. June 2001, Chrudim, Czech Republic

[8] D. Dopheide, D. M. Faber, G. Taux (1989): New Optoelectronic Velocity and Flowrate Measuring Methods using Semiconductor Lasers and Photodiodes. 5th International Conference on Flow Measurement, FLOMEKO '89, 9. - 10. October 1989, Düsseldorf, Conference Proceedings, VDI-Bericht Nr. 768, 1989

[9] D. Dopheide, V. Strunck, E.-A. Krey (1993). Three-component laser Doppler anemometer for gas flow measurements up to 5.500 m3/h. Metrologia, 1993/94, Vol. 30, p. 453–469

[10] B. Harbrink, P. van der Kam; D.King, J.L. De Schutter, V.M. Cannizo: "Perturbation tests on turbine meters" Reprints of the 1995 International Gas Research Conference, 6th – 9th November 1995, Cannes, France, Volume III: Transmission and Storage, Distribution, pp. 456-470

[11] Morrison, G.L.; Hauglie, J.; DeOtte, R.E. Jr. (1995). Beta ratio, axisymmetric flow distortion and swirl effects upon orifice flow meters. Flow Meas. Instr. (6), pp. 207-216

[12] Yeh, T.T.; Mattingly G.E. (1995). Laser Doppler Velocimeter Studies of the Pipe flow Produced by a Generic Header. NIST Technical Note 1409; 79 pages (April 1995)

[13] Voigt, M.: Die Entwicklung von Geschwindigkeits- und Temperaturgrenzschichten in laminaren und turbulenten Kanal- und Rohrströmungen aus asymptotischer Sicht. Fortschritt-Berichte VDI Reihe 7, No. 262. Düsseldorf: VDI-Verlag 1994.

[14] El-Miligui, A.; Cannizaro, F.; Melson, N.D.; von Lavante, E.: A Three Dimensional Multigrid Multiblock Multistage Time Stepping Scheme for the Navier-Stokes Eq. Proc. of 9thGAMM Conf. on Num. Meth. in Fluid Mech., Lausanne, 1991

[15] Hans, V.; Windorfer, H.; von Lavante, E.; Perpéet, S.:Optimization of Acoustic Signals associated with Ultrasound Measurement of Vortex Frequencies. 9th Int. Conf. on Flow Measurement, FLOMEKO, June 15-17, 1998, Sweden

[16] Bradshaw, P.; Fernholz, H.H.; Johnston, J.P.; Woods, J.D.; Reynolds, W.C.; Cebeci, T.; Launder, B.E.; Lumley, J.L.: Turbulence, Topics in Applied Physics, Vol.12. 2nd corrected and updated Ed., Springer-Verlag 1987

[17] Leder, A.: Abgelöste Strömungen, Physikalische Grundlagen. Vieweg-Verlag Braunschweig, Wiesbaden 1992

[18] Harper, R.D.; Jakirlic, S.: Incompressible Recirculating Flows: a Critical Comparison of Computations for Low- and High-Reynolds Number Flow Over a Backward-Facing Step. Notes on Numerical Fluid Mechanics, Dervieux et al. (Eds.), Vieweg 1998, Braunschweig, 65, 141-153

[19] Davidson , L.; P. Nielsen: Study of Low-Reynolds Number Effects in Backward-Facing Step Flow Using Large Eddy Simulations, 6th Int. Conf. on Air Distributions in Rooms, ROOMVENT'98, Eds: E. Mundt & T.G. Malmström Vol. 1, pp. 125-132, Stockholm, Sweden, July 1998.